RSC Advances

ROYAL SOCIETY OF CHEMISTRY

www.rsc.org/advances

On the Properties and Atmospheric Implication of Amine-Hydrated Clusters

Jiao Chen,[1,2] Shuai Jiang,[1] Shou-Kui Miao,[1] Xiu-Qiu Peng,[1] Yan Ma,[1] Chun-Yu Wang,[1] Miao-Miao Zhang,[1] Yi-Rong Liu,[1] Wei Huang[1,2]*

[1]*Laboratory of Atmospheric Physico-Chemistry, Anhui Institute of Optics & Fine Mechanics, Chinese Academy of Sciences, Hefei, Anhui 230031, China*

[2]*School of Environmental Science & Optoelectronic Technology, University of Science and Technology of China, Hefei, Anhui 230026, China*

*E-mail: huangwei6@ustc.edu.cn

Abstract

Amines have been recognized as important precursor species in atmospheric new particle formation. Although Dimethylamine-water clusters have been the focus of a large number of theoretical studies during the last few years, some information regarding these clusters, such as the influence of temperature, the analysis about the weak interaction, and the Rayleigh scatting properties, are still lacking. In this study, The equilibrium geometric structures and thermodynamics of $(CH_3)_2NH(H_2O)_n$ (n=1-6) clusters were systematically investigated using density functional theory (PW91PW91) coupled with the 6-311++G(3df, 3pd) basis set. To confirm the most stable isomer and the order of the different isomers, single-point calculations were executed using a two-point extrapolation method in conjunction with the complete basis set for all isomers. The optimized structures show that the addition of a fifth water molecule changes the most stable configuration from a quasi-planar ring structure to a cage-like configuration. Electron density analysis shows that the interactions of these complexes are mainly medium hydrogen bonds. The temperature

dependence of the conformational population and the Gibbs free energies for the $(CH_3)_2NH(H_2O)_n$ (n=1-6) clusters were performed with respect to temperatures (200-300 K). A weak temperature dependence was found for the formation of $(CH_3)_2NH(H_2O)_n$ (n=1-6) clusters. Dimethylamine hydrated clusters are favorable at low temperatures, but these clusters may difficult to form because of the coupling effect of Gibbs free energies with small negative values and the low relative concentration of Dimethylamine at various atmospheric conditions, and this implies that Dimethylamine-hydrated clusters are difficult to form spontaneously in the atmosphere. Finally, the Rayleigh scatting properties of $(CH_3)_2NH(H_2O)_n$ (n=1-6) have been investigated systematically for the first time.

Ⅰ. Introduction

Atmospheric aerosols are solid or liquid particles suspended in the air that play a key role in direct and indirect effects on the climate[1-5] by altering cloud properties and precipitation. The airborne ultrafine particles in these aerosols adversely affect public health.[6-8] The formation of new particles (NPF) has been observed in a wide range of locations, and is estimated to be an important source of aerosol particles and cloud condensation nuclei. Recently, new particle formations have been observed,[4, 9] however, probing the initial stage of NPF remains a challenge, although the state-of-the-art instruments[9] can measure ionic and neutral clusters. Understanding of the initial formation mechanisms of new particles is still deficient.[10-14]

Neutral binary sulfuric acid-water nucleation[4] and binary ion-induced nucleation[15] have been well studies and serves as an available point of comparison,[16, 17] but it cannot explain new-particle formation events in the atmospheric boundary layer, which indicate that other species must participate to stabilize sulfuric acid particles, such as ions,[15, 18, 19] ammonia and amines[20-27] and organics,[28-33] and iodine oxides.[28] Quantum chemical calculations imply that nucleation with amines is significant favorable over nucleation with ammonia.[34-37] Several experimental studies have confirmed that ammonia and alkyl amines strongly influence nucleation of sulfuric acid and water particles.[16, 17, 22, 38-40] Moreover, recent field observations with gas-phase amine have corroborated that the presence of amines have a considerable effect on new particle formation.[41-44]

Dimethylamine (DMA) is the strongest and most common base in the atmosphere

and it can undergo rapidly acid-base reactions that enhances neutral and ion-induced sulfuric acid-water nucleation.[36, 40, 41, 45] Recently filed studies have shown a correlation between new particle formation and the presence of DMA.[38, 46-49] Experiments[38] using the CLOUD chamber at CERN confirmed that concentration of DMA exceeding three parts per trillion by volume was able to enhance new particle formation rates more than 1,000-fold compared to ammonia.

Hydrogen bonding interactions are the driving forces for the formation of atmospheric molecular complexes, whose strength determines the thermodynamic stability of these complexes. Some Quantum chemical studies of sulfuric acid and DMA and water have been performed,[34-36, 50] but the analysis about the weak attraction in the clusters which is essential for their nucleate mechanism is still vacant. The theory of atoms in molecules (AIM), developed by Bader and coworkers[51] is a precious tool for understanding hydrogen bonds in molecular complexes. There are a number of studies dealing with sulfuric acid-DMA-water system that show how DMA will not form clusters with water.[37, 50, 52, 53] All of these researches were calculated at constant temperature and 1 atm. As we all know, temperature dependence of thermodynamical properties is a significant parameter for understanding how a specific nucleation mechanism plays role in NPF. Furthermore, climate was affected by aerosols directly by scattering the light from the sun.[54] Although Rayleigh scattering properties of large particles are well understood, the Rayleigh scattering properties of clusters, especially at the molecular level, are still not covered. Considering all of these, AIM analysis, temperature correlation and Rayleigh

scattering properties were performed for the first time in this study for the clusters of $(CH_3)_2NH(H_2O)_{1-6}$.

This study include some aspects: (1) Basin-Hopping (BH) was coupled with density functional theory (DFT) and used to determine the global and local minima by sampling the potential energy surface thoroughly; (2) single-point calculations were executed using a two-point extrapolation method in conjunction with the complete basis set for all isomers; (3) electron density analysis was performed to investigate the interactions of these complexes; (4) the temperature dependence of the conformational population and the Gibbs free energies for the $(CH_3)_2NH(H_2O)_{1-6}$ clusters were investigated; (5) the Rayleigh scattering properties of $(CH_3)_2NH(H_2O)_{1-6}$ have been investigated systematically for the first time.

Ⅱ. Computational Methods

As the number of water molecules increases, the number of isomers increases tremendously, and the most stable conformers become sophisticated and not obvious. Thus, searching for large clusters by chemical intuition is very difficult. To overcome this problem, the BH algorithm[55-58] was employed, which has been successfully applied to atomic clusters.[58-63] In order to effectively search molecular cluster, the BH algorithm using compressed sampling technique was improved in previous study, such as the structures of $(H_2O)_n$ (n=4-10) clusters,[64] CH_3NH_2-H_2O clusters,[65] $Cl^-(H_2O)$ clusters,[66, 67] H_2SO_4-$C_2H_2O_4$-H_2O clusters[68] and so on.[69-71] The BH method includes two steps: First, a new structure is generated via the random displacement of atoms; then, the structure is optimized to the local minimum. Second, this local energy

minimum is used as a criterion to accept the initial generated structure spaces with Boltzmann weight at a finite temperature. The initial geometries were obtained with BH algorithm, and PW91/DND implemented in DMol^3 software package[72] was employed in the DFT module coupled with BH. Then the stable isomers within 10 kcal/mol of the stable global minimum were optimized at PW91PW91/6-311++G(3df,3pd) method. For each stationary point, frequency calculations have been operated to ensure there were no imaginary frequencies. And the convergence standards used for the optimization are default setting in Gaussian09 software.[73] At the standard state of 1 atm of pressure and 298K, the binding energies, enthalpies, and Gibbs free energies were computed for all of the selected clusters using the harmonic oscillator and rigid rotor approximations. The structural information (bond lengths) was provided with Chemcraft 1.6 (http://www.chemcraftprog.com).

Previous studies have indicated that PW91PW91/6-311++G(3df,3pd) provides better performance for predicting the vibrational spectrum of oxalic acid than MP2/6-311++G(3df,3pd) or B3LYP/6-311++G(3df,3pd).[32, 33, 74, 75] Moreover, it is found that the PW91PW91 method well reproduces the MP2 and CCSD(T) results of the first hydration sulfuric acid.[76] However, one of the main sources of error in quantum chemistry calculations is that the basis set is not sufficiently larger, or it is far from the complete basis set limit. Using PW91PW91 with a finite basis set for the calculation of the interaction energies of hydrogen bonds systems encounters a problem called the basis set superposition error (BSSE). To reduce this error, and the

calculation cost, extrapolating the energy to the complete basis set (CBS)[77] limit was performed on the single point energy calculated using the method of DF-MP2-F12. The CBS limit was estimated with a two-point extrapolation scheme.[78, 79] The equations for the corresponding calculations are as follows:

$$E_{CBS}^{SCF} = E_{N}^{SCF} + B*EXP(-AN) \quad (1)$$

$$E_{CBS}^{corr} = \frac{N^3 E_N^{corr} - (N-1)^3 E_{N-1}^{corr}}{N^3 - (N-1)^3}$$

$$E_{CBS}^{RI-MP2} = E_{CBS}^{SCF} + E_{CBS}^{corr}$$

Here A and B are the fitting parameters and E_{CBS}^{SCF}, E_{CBS}^{corr}, E_{CBS}^{RI-MP2} are the SCF, correlation and total energy, respectively. All of the calculations were performed using Molpro 2010.1.[80] and the default convergence criteria were defined in Molpro 2010.1.

Although DFT-methods can qualitatively describe the geometries and vibrational frequencies, the weak interactions arising from dispersion forces are unable be accurately treated, which plays a moderately important role in hydrogen bonding. Two main pathways are provided to obtain accurate thermochemistry for hydrogen-bonded clusters. One method is to use DFT which are sufficiently parameterized to replicate binding energies of various benchmarking sets of weak interactions clusters, although the inaccurate treatment of dispersion. Another alternative is to use correlated wavefunction-based methods such as MP perturbation theory or coupled-cluster methods. However, the computational cost of the correlated wavefunction-based method is generally orders of magnitude more than that of DFT methods. Here, extrapolation is performed on DF-MP2-F12 calculated energy values to reduce basis-set superposition errors and basis-set incompleteness errors. The study by

Temelso et al.[81] showed that the convergence of the binding energy to the CBS is not monotonic due to the incompleteness of the AVDE basis set resulting in an overestimation of the binding energy. Hill[82] demonstrated that MP2-F12 method combining with the cc-pV*n*Z-F12 basis set produces results that are approximately equal to MP2-F12/aug-cc-pV(*n*+1)Z. Aug-sets include additional diffuse higher angular momentum functions, which lead to significantly more basis set superposition error than the cc-pV*n*Z-F12 basis set. Another important problem is the calculation of energies for larger clusters where the computational costs prohibit the use of large basis sets. Recent work illustrated that the binding energies from DF-MP2-F12/VQZ-F12 are close to the basis set limit.[83] To assure the accuracy without paying too much calculation cost, we selected DF-MP2-F12/ cc-pV*n*Z (n=D, T) for the extrapolation scheme.

Two-point extrapolation with conventional scheme (equation 1) was carried out by applying the cc-pVDZ-F12 and cc-pVTZ-F12 basis set coupled with DF-MP2-F12 for calculating the SCF and the correlation energy in this work. To obtain the fitting parameter A, which is a constant based on equation (1), the binding energies for the six isomers of $(CH_3)_2NH(H_2O)_{n=1-3}$ were calculated at the DF-MP2-F12/cc-pV*n*Z-F12 (*n* = D, T, Q) level of theory. A three-point extrapolation was performed to fit the constant A, which is approximately equal to 1.48.

Figure 1 shows that the convergence of the binding energy is monotonic, systematic convergence of the energies toward the CBS limit is again a feature of these basis sets. The two-point extrapolation scheme for the binding energy deviates

from the benchmark DF-MP2-F12/VQZ-F12 with the difference increasing from 1.14 to 1.77 kcal/mol as the clusters size grows. Thus, the deviation monotonously increases, indicating that as the number of water molecules grows, the difference will increase correspondingly. For the $(CH_3)_2NH(H_2O)_2$ and $(CH_3)_2NH(H_2O)_5$ clusters, the geometry of the most stable isomers optimized with the PW91PW91/6-311++G(3df, 3pd) method was 2b and 5d, respectively. For the DF-MP2-F12/CBS// PW91PW91/6-311++G(3df, 3pd) level, 2a and 5a were found to be the global minimum. Furthermore, the isomers with the same number of water molecules were arranged in order of increasing electronic energy. The difference in the calculated binding energies between CBS and DF-MP2-F12/cc-VTZ-F12 is several kcal/mol, and with the cluster size increasing, the errors in the Gibbs free energy for the same magnitude of binding energy will generate a tremendous effect on quantities such as cluster abundance and the nucleation rates because they depend exponentially on the nucleation barriers.

Based on the global minima of $(CH_3)_2NH(H_2O)_n$(n=1-6) obtained in this work, optical properties of the pre-nucleation clusters were evaluated. Light scattering intensities and the isotropic mean polarizabilities $\bar{\alpha}$ as well as anisotropic polarizabilities $\Delta\alpha$ were calculated at CAM-B3LYP/aug-cc-pVDZ level of theory and the relevant computation methods have been given in our earlier study.[66] The benchmark for the smallest clusters of H_2SO_4-NH_3-H_2O were performed by Elm.[84] They found that CAM-B3LYP/aug-cc-pVDZ was a good balance between efficiency and accuracy, obtaining good agreement with both experimental and CCSD(T) values

of the polarizability. In this article, to find an appropriate methodology to calculating the optical properties of the DMA-H_2O clusters, five different DFT functionals with the aug-cc-pVDZ basis sets was performed. The results are shown in Table 1, analyzed the results, CAM-B3LYP/aug-cc-pVDZ was confirmed to be a good suitable method, which yielding good agreement with the MP2 values of the polarizability.

Ⅲ. Results and Discussions

To understand the initial steps of the formation of new particles when DMA participate in forming new particle, we first performed the quantum chemical calculation for $(CH_3)_2NH(H_2O)_n$(n=1-6) to search for the global minimum and several local minima. All of the hydrated clusters with the same number of water molecules were arranged according to the binding energy with the ZPE correction from lowest to highest. The complexes were marked by na, nb, nc, *etc*., where n is the number of water molecules in the $(CH_3)_2NH(H_2O)_n$ clusters.

3.1 Structures

Monohydrates In our search for the global and low-lying local minima of $(CH_3)_2NH(H_2O)_1$ clusters, two structures shown in Figure 2 were found to be the global minimum and local minimum in energy. According to Nadykto et al.,[35] isomer 1b was reported as the most stable isomer. The high-level calculation at the DF-MP2-F12/CBS// PW91PW91/6-311++G(3df, 3pd) level showed that 1a was the lowest structure.

Dihydrates In our search for the global minimum of the $(CH_3)_2NH(H_2O)_2$ cluster, the ground-state geometry of isomer 2b shown in Figure 2 is optimized at the

PW91PW91/6-311++G(3df, 3pd) level, which agrees with the previous result.[35] We calibrated the single-point energy at the DF-MP2-F12/CBS//PW91PW91/6-311++G(3df, 3pd) level. Configuration 2b is the second lowest-energy structure, which is higher in energy by 0.24 kcal/mol than 2a.

Trihydrates Eight isomers were taken into account (in Figure 2). According to the arrangement, there are two types of pattern in the cyclic forms. The three lowest-energy isomers (3a, 3b and 3c) are similar and have four-membered ring structures with four HBs. The atoms forming the HB network nearly lie in the same plane, and the difference in the orientation of the three isomers is due to the free hydrogen atoms. Thus, the binding energies are very similar. For the other five isomers, three water molecules form a coplanar three-membered ring structure, except for the free hydrogen atoms. The orientation of the free hydrogen atoms and the three-membered ring gives rise to the difference in the structure and the binding energies. For the first type, the computed binding energies with the zero-point energy correction for each structure has a small gap comparing with the most stable structure the energy separation is 0.12 kcal/mol, 0.39 kcal/mol. In contrast, a wide gap exists between the two types on the binding energies, ranging from 2.79 kcal/mol to 3.80 kcal/mol. This gap means that the four-membered ring structure is more stable than the three-membered ring structure. The structure of 3a are similar with the global minimum of the $(H_2O)_4$ cluster[85].

Tetrahydrates The most stable configuration (4a) for $(CH_3)_2NH(H_2O)_4$ clusters is a ring structure with five H-bonds, which is similar to the cluster of

$(H_2O)_5$.[85] The HB length of N-H···O is 1.909 Å, and this is weaker than others (1.643 Å, 1.644 Å, 1.667 Å, and 1.702 Å). Interestingly, with the orientation of the free hydrogen changing, the configurations labeled 4b and 4e became distorted and no longer planar. The clusters change from planar to contorted planar to minimize repulsions from the adjacent hydrogens. For 4h and 4i, four water molecules form a four-membered ring with similar features to the trihydra tes. In addition to the single ring structures, three bicyclic structures (4d, 4f, 4g and 4j) are observed. Detailed information about these structures is shown in Figure 3.

Pentahydrates For the case of the $(CH_3)_2NH(H_2O)_5$ cluster in Figure 4, eighteen low-lying isomers within 4 kcal/mol were selected. Compared with the trihydrates and tetrahydrates clusters, the fifth water molecule produces a significant change in the most stable structure, changing it from a planar ring to a three-dimensional form. For the pentahydrate clusters, the most stable structure is a prism structure lacking one side with eight H-bonds, while it is a complete prism structure for the $(H_2O)_6$ cluster.[85] The 5b geometry is closest to 5a, although its binding energy lies higher by 0.85 kcal/mol. The orientation of the free hydrogen and the relative orientation between DMA and hydrated ring structures make the conformation different. The binding energies of these similar isomers have small gaps that are within a kcal/mol. Many configurations are derived from $(CH_3)_2NH(H_2O)_4$ clusters. For instance, 5i is a derivative of the existing structure 4h by the addition of H_2O and with minor rearrangements to the existing network of HBs. Similarly, 5e is a derivative of 4d. The frequency calculation performed on 5k shows that it has one

imaginary frequency of 3.15. This imaginary frequency is so small that the geometry can be considered a local-minimal structure.

Hexahydrates Among the stable isomers of the $(CH_3)_2NH(H_2O)_6$ cluster in Figure 5, isomer 6a is the lowest-energy structure, and was derived from isomer 5a with one water molecule inserted into the existing HB network and then forming a non-planar four-membered ring. The second most stable structure (6b), has a slightly distorted, cube-like structure with a corner missing and is similar to the most stable $(H_2O)_7$ cluster.[85] Although structures 6b and 6d are similar to 6a, which is derived from 5a, a considerable discrepancy was generated because the sixth water molecule embeds in a different position as compared to isomer 5a. Our calculation of the binding energies for 6a and 6b without ZPE correction (in Table 3) show that 6a lies slightly higher than 6b by 0.27 kcal/mol. Due to HB formation between amino hydrogen atom and the oxygen atom of a water molecule, 6c, 6e and 6h are all polycyclic structures with nine H-bonds. When the amino hydrogen atom is free, different kinds of polycyclic structures (6i, 6k and 6l) were composed of six water molecules. In addition to the polycyclic structures, there are many bicyclic structures such as 6j with eight H-bonds.

3.2 Electron Density Analysis

The intermolecular interaction distances are just below the sum of the van der Waals radii of atoms naturally, they cannot be used to identify the strength of hydrogen bonds and the nature of any possible bonding between the methyl and water molecules, even for revealing the steric interactions. Then, AIM theory provided by

the topological analysis of the electron density was performed here to deepen understanding of the intermolecular hydrogen bond of the most stable conformations. The basis of the topological parameters at the bond critical points (BCPs) was calculated based on Bader's atoms in molecules theory.[51] Some representatives for this kind of interaction were chosen, such as the electron density ρ, the Laplacian of the electron density $\nabla^2\rho$, the kinetic electron energy density G, the potential density V, the electron energy density H, and the G/|V| at the bond critical point. The values of $\nabla^2\rho$ and H indicate the nature of the interaction, and a negative value of $\nabla^2\rho$ presents that there is a shared interaction like in a covalent bond, whereas a positive value indicates closed-shell system interactions, such as HB，van der Waals forces. Furthermore, the energy density has proved to be more appropriate and sensible index than $\nabla^2\rho$ to characterize the strength of hydrogen bonds. Thus, both $\nabla^2\rho$ and H > 0 represent weak HB, and $\nabla^2\rho$ >0 and H < 0 show medium HB, while both $\nabla^2\rho$ and H < 0 show strong HB. Moreover, G/|V| taken as the balance between the positive value of G and negative value of V may indicate the bonds corresponding to covalent or non-covalent interaction. Thus, if G/|V| is greater than 1, the interaction characters as closed-shell non-covalent interactions. If the ratio is between 0.5 and 1, the interaction displays partly covalent interactions in nature, and if less than 0.5, the interaction is a shared covalent interaction.

From Table S1, it is observed that the values of $\nabla^2\rho$ of the most stable conformations at the BCPs are all positive except for O5-H14···O2 of isomer 6a. All the O-H···N show medium HBs with H<0 and their corresponding values of $\nabla^2\rho$

decay with increasing water molecules up to five in the range of 0.0735-0.0051 a.u., while $\nabla^2\rho$ has a big step increase as for 6a. For isomer 2a, C-H6···O2 and C-H7···O2 are both non-covalent because the values of G/|V| are greater than 1. In the case of 3a and 6a, the HB formation between the amino hydrogen atom and the oxygen atom of a water molecule are both non-covalent. For 4a, all of the HBs are medium HBs. For 5a, except for the HBs of C-H13···O3, O2-H11···O6 and O4-H15···O6, other HBs of this structure display the characteristics of medium HBs. As the water molecules up to six, a strong HB of O5-H14···O2 was observed.

The non-covalent interactions (NCI) analysis method derived from the correlation between the reduced density gradient and the electron density has been studied by Yang.[86, 87] The reduced density gradient

$$s = \frac{1}{2(3\pi^2)^{1/3}} \frac{\nabla\rho}{\rho^{4/3}}$$

is a fundamental dimensionless quantity in DFT presented to describe the deviation from a homogeneous electron distribution.[86] To a certain extent, the NCI analysis can be regarded as an extension of AIM.[87] Not only can the location of the pairwise atoms connected along the bond path be identified, the properties around BCPs can be visualized using NCI. The reduced density gradient is able to be used to confirm the covalent interactions and the noncovalent interactions in real space.[88]

Figure 6 shown the reduced gradient isosurfaces (s=0.5 a.u.) using Multiwfn program[89] and VMD program.[90] The green to blue color regions of the binding isosurface indicate that the HB interaction is becoming stronger. HB consist of ammonia nitrogen and hydrogen atoms of water molecule is the most strong HB for

every conformation and the strength become more strong as the number of water molecules increasing. At the same time, steric hindrance cannot be neglected because of the two methyl groups. Furthermore, repulsions located at the center of H-bonds ring are very weak, and the more H-bonds forming ring, the weaker of the repulsion. Even though, there is medium hydrogen interaction building up between DMA and water molecules, which is not substantial enough to come across the energy barrier for plotting the reaction of hydration spontaneously at the standard state of 1atm of pressure and 298K.

3.3 Thermodynamics of $(CH_3)_2NH(H_2O)_n$ Formation

The binding energies ΔE(kcal/mol) of the clusters were calculated using the following equation. The ZPE-corrected binding energies ΔE+ZPE(kcal/mol), the interaction enthalpies ΔH(kcal/mol) and Gibbs free energies changes ΔG(kcal/mol) ware calculated in the same way:

$$\Delta E_{(CH_3)_2NH(H_2O)_n} = E_{(CH_3)_2NH(H_2O)_n} - E_{(CH_3)_2NH(H_2O)_{n-1}} - E_{H_2O}$$

Table 2 and 3 show the thermodynamics of the most stable configurations at the DF-MP2-F12/CBS level of theory upon adding a water monomer to the most stable $(CH_3)_2NH(H_2O)_{n-1}$ cluster to form $(CH_3)_2NH(H_2O)_n$ clusters ΔE(kcal/mol), ΔE+ZPE(kcal/mol), ΔH(kcal/mol) and ΔG(kcal/mol) were calculated, respectively.

Figure 7 presents how the binding energy, enthalpy and Gibbs free energy of the global minimum changed with the growing cluster size. The change in the binding energy is non-monotonic, and the binding energy with the ZPE correction ranges from -5.63 to -10.88 kcal/mol by the stepwise addition of water monomers. As one to three

water molecules are added, the binding energy becomes more negative gradually because new ring hydrogen bonds are formed. In the case of $(CH_3)_2NH(H_2O)_4$ cluster, this tendency is reverted and appears to be a maximum rise in the stepwise hydration. By adding the fifth water, the relative stabilization is increased as the conformation varies from 2-dimensional to 3-dimensional. In the case of $(CH_3)_2NH(H_2O)_6$ cluster, the binding energy rapidly decreases and appears to be a minima dip in the stepwise hydration. This discrepancy resulted from the differences among the most stable conformations. The results showed that the stability of the clusters varies, and the discrepancies rely on (a) the number of H-bonds, (b) the network of H-bonds, (c) the configuration of the isomers (e.g. quasi-planar, distortion-planar and three-dimensional), (d) whether the amino nitrogen atom is involved in bonding hydrogen bond and (e) the orientation of free hydrogen atoms. These factors determine which isomer is the global minimum. The non-monotonic change for enthalpy is similar with the variation of binding energy with the ZPE correction.

The non-monotonic change in ΔG with the addition of each successive water molecule (Figure 7) is different from the change in the binding energy. For $(CH_3)_2NH(H_2O)_{n=3}$, the most stable structure corresponding to the ΔG is minimized, and the maximum Gibbs energy of interaction is achieved when the fifth water molecule is added. Table 2 and 3 presented that all of the reactions involving the addition of water monomer are slightly exothermal. Due to the kinds of HB networks and the distance of HBs, there is no absolute correlation between the enthalpy contribution and the number of the hydrogen bonds. The addition of more water

molecules results in a cage of more H-bonds, and in most cases, the lowest-free-energy structures have the fewest number of H-bonds because of entropic cost. To this point, clusters with up to six water molecules have been discussed. Thermodynamically, the formation of these structures is clearly unfavorable. The magic number of water molecules that thermodynamically favored remains unknown. Because of the positive free energy, the equilibrium hydrate distributions are very small, and these clusters cannot form spontaneously at 298K, 1atm. Nevertheless, this study can act as a reference for the study of ternary nucleation systems containing DMA, sulfuric acid and water molecules. The study by Xu[33] shown that, though the formation of DMA hydration is not favorable, the formation of H_2SO_4-DMA-$(H_2O)_n$ clusters is more favorable through the collision between the H_2SO_4 and DMA-$(H_2O)_n$ clusters than the H_2SO_4-$(H_2O)_n$ clusters and DMA, and more water molecules, more favored.

3.4 Temperature Dependence of the Conformational Population and Gibbs Free Energy

The contribution from the global minimum is important for the ensemble of energetically accessible conformations because of its largest population. However, as the cluster systems are becoming larger and the configurations more complex, the energetic difference between the global minimum and low local minima is getting smaller due to the flexible HB networks. These results indicate that the local minima might be significant as the larger weight. The temperature dependence of the thermodynamics is also an important parameter that could change the stability order

of the global minimum and the local minimum as well as the weight of the isomers. Thus, the effects of the temperature on the lower local minima contributions were investigated in this work, which could give insight into the relative stabilities of the different isomers. The relevant computation methods have been given in our earlier study.[70]

The variation of the population of the isomers versus the temperature is presented in Figure 8. For $(CH_3)_2NH(H_2O)_1$, the global minimum proportion of 1a is less than isomer 1b, and as the temperature increases, the weight of 1b increases monotontically. The difference between the two isomers gradually increases. Figure 8a shows the results of $(CH_3)_2NH(H_2O)_2$ clusters. The weight of the global minimum 2a decreases slightly from 212.6 to 249.9 K, reaching the maximum of 62.92% and then decreasing to the minimum of 60.01% at 298.15K. In the case of n=3, 3b has the largest proportion and increases slowly for the entire time. Moreover, the total population of 3a, 3b and 3c is approximately 100%, indicating a cyclic structure with four H-bonds is the most stable structure for trihydrates. Figure 8c presents the conformational population of isomers for n=4. The populations of the local minimum increase while the global minimum decreases monotonically with the temperature increases. The strong entropy effect could be seen in 4h for the population with the largest entropy. For the case of n=5 given in Figure 8d, our results predict a monotonic increase for 5i, 5l, 5m with respect to temperature. The growth rate of 5l is clearly larger than the other isomers, and 5l has the largest proportion above the temperature 259.3 K, which indicates that planar structures have a leading role at high

temperature. The populations of 5d and 5a drop slightly and significantly, respectively. However, 5d is more weighted than 5a as the temperature increases. The weights for other isomers almost remain constant, and their proportions are too small, so be negligible. In the case of n=6, the global minimum weight is the largest among all of the isomers in the temperature range from 212.6 to 298.15 K. Similarly, 6a decreased dramatically from 72.44% to 35.39%. The local minima, except for isomer 6b, increase as the temperature increases. In conclusion, the weight of the global minima and local minima change as the temperature increase. The effects of temperature could contribute to the alternation of the stability order of the isomers.

The temperature dependence of Gibbs free energy for the formation of $(CH_3)_2NH(H_2O)_{n=1-6}$ clusters with respect to different temperature (200-300 K) was investigated. Figure 9 shows the minimum thermodynamics of stepwise hydration of $(CH_3)_2NH(H_2O)_{n=1-6}$. There is a strong temperature dependence for $(CH_3)_2NH(H_2O)_{n=1-6}$ cluster formation. The lowest free energy shift from n=6 below 223.7 K to n=3 around the temperature of 230K. As the temperature falls below 223.7 K, the stepwise addition of water molecules from one to six into DMA clusters is favorable. As the temperature increases, the clusters are less favorable, and as the temperature reaches 298.15 K, all of the clusters become unfavorable. According to Kim,[91] it is easy to change the stabilities of the clusters containing multiple hydrogen bonds when the temperature rises, which is a result of the entropy effect. Although DMA hydrated clusters are favorable at low temperatures, these clusters could not form because of the coupling effect of Gibbs free energies with small negative value

and the low relative concentration of DMA at various atmospheric conditions.

3.5 Optical Properties

Aerosols weaken light by absorbing and scattering and the extinction properties have a great effect on atmospheric visibility and radiative forcing.[92, 93] Rayleigh scattering is the principle scattering for molecules, clusters, and small particles with diameters much smaller than the wavelength of the light. Although Rayleigh scattering properties of large particles are well understood, the Rayleigh scattering properties of clusters, especially at the molecular level, are still not covered. In this work, Rayleigh scattering properties of $(CH_3)_2NH(H_2O)_{n=1-6}$ clusters were investigated for the first time.

The small clusters with up to six water molecules yield slightly higher binding isotropic mean polarizabilities $\bar{\alpha}_{Binding}$ in the range of -0.02 to 2.43 a.u. as shown in Table S2, which is attributed to the small hydrogen bonding network as the number of water molecules within 6. The isotropic mean polarizabilities $\bar{\alpha}$ are quite dependent on the water number and vary linearly as shown in Figure 10a, similarly to the study of methanol clusters[94] and chloridion hydration systems,[66] and they increase drastically from 47.78 to 96.86 a.u.. From Figure 10b, it is quite clearly observed that the Rayleigh scattering intensities of natural light $\mathcal{R}_n$ dramatically increases with the number of water molecules increasing following the trend of a second order polynomial with correlation coefficient 0.99919. This increasing trend can be attributed to the gradually increasing isotropic mean polarizabilities $\bar{\alpha}$ which will dominate the Rayleigh scattering.

From Figure 10c and 10d, the anisotropic polarizabilities Δα and the depolarization ratios of natural light σ_n of the $(CH_3)_2NH(H_2O)_{n=1-6}$ clusters can be seen as the number of water molecules in the clusters. It is observed that anisotropic polarizabilities Δα decrease from a monomer to dimer and then increases from a dimer to tetramer. In the case of $(CH_3)_2NH(H_2O)_{5-6}$, Δα decay slightly then decrease with a big step from a pentamer to a hexamer. The calculated depolarization ratio of natural light σ_n has the similar variation trend with anisotropic polarizabilities Δα, which is due to an increase in the isotropic mean polarizabilities $\bar{\alpha}$ in combination with the anisotropic polarizability Δα which plays the leading role and has the positive correlation with σ_n. In Figure 2-5, it is obviously seen that clusters become a quasi-planar ring structures as the addition of a second water molecules, nevertheless, conformation changes to be a cage-like three-dimensional structure for pentamer. So this is consistent with what is to be expected as the cluster change from a molecular cluster into a spherical isotropic particle.

Observation by Elm *et.al*[84] who studied the Rayleigh scattering properties of atmospheric pre-nucleation systems found that all different conformations within each cluster yield very similar isotropic mean polarizabilities $\bar{\alpha}$ within 2 a.u.. While from other studies[94, 95] of Rayleigh scattering properties, the remarkable differences among different conformations have been studied, which indicate that anisotropic polarizability Δα and depolarization ratio σ could be alternative parameters depend on the constituents and conformations. In our study for the ten isomers of $(CH_3)_2NH(H_2O)_5$, it is observed that even though 5a, 5c, 5e, 5h, 5i, 5j present

different hydrogen bonding network with various N-H and O-H hydrogen bonding numbers, the $\bar{\alpha}_{Binding}$ difference among these isomers is rather small within 3 a.u. as shown in Table S2, which is smaller for the isomers 5c, 5d, 5f, 5g with the same bonding pattern. And for depolarization ratios of $(CH_3)_2NH(H_2O)_5$, the case is similar. So these could imply that the anisotropic polarizability and depolarization ratio cannot be regarded as the alterative parameters at least for the DMA hydration clusters, which is similar to the case of methanol[94] and chloridion hydration systems.[66] While the anisotropic polarizabilities $\Delta\alpha_{Binding}$ are much isomer dependent fluctuated from -3.49 to 0.79 a.u. for the ten isomers of $(CH_3)_2NH(H_2O)_5$, which has been observed in sulfuric acid hydration systems.[84]

4. Conclusions

We have investigated the structure evolution, non-covalent Interactions, temperature effects, and optical properties of hydrated DMA clusters. The global and low-lying local minima isomers were optimized at PW91PW91/6-311++G(3df, 3pd) level. The thermodynamics properties were further corrected using DF-MP2-F12/CBS// PW91PW91/6-311++G(3df, 3pd). Electron density analysis shows that the interactions of these complexes are mainly medium hydrogen bonds, but not substantial enough to come across the energy barrier for plotting the reaction of hydration spontaneously at the standard state of 1atm of pressure and 298K. The temperature dependence of the conformational population and the Gibbs free energy for the formation of $(CH_3)_2NH(H_2O)_{n=1-6}$ clusters were investigated. A weak temperature dependence was found for the formation of $(CH_3)_2NH(H_2O)_{n=1-6}$ clusters.

DMA hydrated clusters are favorable with negative values at low temperatures, especially for $(CH_3)_2NH(H_2O)_3$ but these clusters may difficult to form because of the coupling effect of Gibbs free energies with small negative values and the low relative concentration of DMA at various atmospheric conditions. And this implies that DMA-hydrated clusters are difficult to form spontaneously in the atmosphere. Finally, the Rayleigh scatting properties have been investigated. It comes out that the isotropic mean polarizabilities show a linear relation while the Rayleigh scatting intensities of nature light follow the second order polynomial trend as the clusters size increasing. Furthermore, the anisotropic polarizability and depolarization ratio cannot be regarded as the alterative parameters at least for the DMA hydration cluster. The large hydrated DMA clusters need further study and this study could also provide help for the study of ternary nucleation systems containing DMA, sulfuric acid and water molecules.

Acknowledgments

The study was supported by grants from the National Natural Science Foundation of China (Grant No. 21403244 and 21133008), the National High Technology Research and Development Program of China (863 Program) (Grant No. 2014AA06A501). Acknowledgement is also made to the "Thousand Youth Talents Plan", Scientific Research Equipment Development Program (YZ201422) and "Interdisciplinary and Cooperative Team" of CAS. The computation was performed in EMSL, a national scientific user facility sponsored by the department of Energy's Office of Biological and Environmental Research and located at Pacific Northwest National Laboratory (PNNL). PNNL is a multiprogram national laboratory operated

for the DOE by Battelle. Part of the computation was performed at the Supercomputing Center of USTC.

Reference

1 R. Makkonen, A. Asmi, V.-M. Kerminen, M. Boy, A. Arneth, P. Hari and M. Kulmala, *Atmos. Chem. Phys.*, 2012, **12**, 1515-1524.

2 J. Kazil, P. Stier, K. Zhang, J. Quaas, S. Kinne, D. O'Donnell, S. Rast, M. Esch, S. Ferrachat, U. Lohmann and J. Feichter, *Atmos. Chem. Phys.*, 2010, **10**, 10733-10752.

3 M. B. Baker and T. Peter, *Nature*, 2008, **451**, 299-300.

4 M. Kulmala, H. Vehkamäki, T. Petäjä, M. Dal Maso, A. Lauri, V.-M. Kerminen, W. Birmili and P. H. McMurry, *J. Aerosol Sci.*, 2004, **35**, 143-176.

5 R. J. Charlson, J. H. Seinfeld, A. Nenes, M. Kulmala, A. Laaksonen and M. C. Facchini, *Science*, 2001, **292**, 2025-2026.

6 A. Saxon and D. Diaz-Sanchez, *Nat. Immunol.*, 2005, **6**, 223-226.

7 G. Oberdörster and M. J. Utell, *Environ. Health Perspect.*, 2002, **110**, A440.

8 P. Penttinen, K. Timonen, P. Tiittanen, A. Mirme, J. Ruuskanen and J. Pekkanen, *Eur. Respir. J.*, 2001, **17**, 428-435.

9 M. Kulmala, J. Kontkanen, H. Junninen, K. Lehtipalo, H. E. Manninen, T. Nieminen, T. Petaja, M. Sipila, S. Schobesberger, P. Rantala, A. Franchin, T. Jokinen, E. Jarvinen, M. Aijala, J. Kangasluoma, J. Hakala, P. P. Aalto, P. Paasonen, J. Mikkila, J. Vanhanen, J. Aalto, H. Hakola, U. Makkonen, T. Ruuskanen, R. L. Mauldin, J. Duplissy, H. Vehkamaki, J. Back, A. Kortelainen, I. Riipinen, T. Kurten, M. V. Johnston, J. N. Smith, M. Ehn, T. F. Mentel, K. E. J. Lehtinen, A. Laaksonen, V. M. Kerminen and D. R. Worsnop, *Science*, 2013, **339**, 943-946.

10 J. Vanhanen, J. Mikkilä, K. Lehtipalo, M. Sipilä, H. Manninen, E. Siivola, T. Petäjä and M. Kulmala, *Aerosol Sci. and Tech.*, 2011, **45**, 533-542.

11 T. Petäjä, M. Sipilä, P. Paasonen, T. Nieminen, T. Kurtén, I. K. Ortega, F. Stratmann, H. Vehkamäki, T. Berndt and M. Kulmala, *Phys. Rev. Lett.*, 2011, **106**, 228302.

12 A. Hirsikko, T. Nieminen, S. Gagné, K. Lehtipalo, H. Manninen, M. Ehn, U. Horrak, V.-M. Kerminen, L. Laakso and P. McMurry, *Atmos. Chem. Phys.*, 2011, **11**, 767-798.

13 M. Sipilä, T. Berndt, T. Petäjä, D. Brus, J. Vanhanen, F. Stratmann, J. Patokoski, R. L. Mauldin, A.-P. Hyvärinen and H. Lihavainen, *Science*, 2010, **327**, 1243-1246.

14 M. Sipilä, K. Lehtipalo, M. Attoui, K. Neitola, T. Petäjä, P. Aalto, C. O'Dowd and M. Kulmala, *Aerosol Sci. and Tech.*, 2009, **43**, 126-135.

15 E. Lovejoy, J. Curtius and K. Froyd, *J. Geophys. Res. Atmos. (1984–2012)*, 2004, **109**, D08204.

16 J. Kirkby, J. Curtius, J. Almeida, E. Dunne, J. Duplissy, S. Ehrhart, A. Franchin, S. Gagné, L. Ickes and A. Kürten, *Nature*, 2011, **476**, 429-433.

17 J. Zollner, W. Glasoe, B. Panta, K. Carlson, P. McMurry and D. Hanson, *Atmos. Chem. Phys.*, 2012, **12**, 4399-4411.

18 F. Yu, *Atmos. Chem. Phys.*, 2006, **6**, 5193-5211.

19 F. Yu and R. P. Turco, *Geophys. Res. Lett.*, 2000, **27**, 883-886.

20 J. Herb, Y. Xu, F. Yu and A. Nadykto, *J. Phys. Chem. A*, 2012, **117**, 133-152.

21 M. E. Erupe, A. A. Viggiano and S. H. Lee, *Atmos. Chem. Phys.*, 2011, **11**, 4767-4775.

22 D. R. Benson, J. H. Yu, A. Markovich and S. H. Lee, *Atmos. Chem. Phys.*, 2011, **11**, 4755-4766.

23 D. R. Benson, L. H. Young, F. R. Kameel and S. H. Lee, *Geophys. Res. Lett.*, 2008, **35**, L11801.

24 T. Kurtén, L. Torpo, C. G. Ding, H. Vehkamäki, M. R. Sundberg, K. Laasonen and M. Kulmala, *J. Geophys. Res. Atmos. (1984–2012)*, 2007, **112**, D04210.

25 N. Bork, J. Elm, T. Olenius and H. Vehkamäki, *Atmos. Chem. Phys.*, 2014, **14**, 12023-12030.
26 J. W. DePalma, D. J. Doren and M. V. Johnston, *J. Phys. Chem. A*, 2014, **118**, 5464-5473.
27 I. Ortega, T. Olenius, O. Kupiainen-Määttä, V. Loukonen, T. Kurtén and H. Vehkamäki, *Atmos. Chem. Phys.*, 2014, **14**, 7995-8007.
28 R. Zhang, A. Khalizov, L. Wang, M. Hu and W. Xu, *Chem. Rev.*, 2011, **112**, 1957-2011.
29 R. Zhang, *Science*, 2010, **328**, 1366-1367.
30 R. Zhang, I. Suh, J. Zhao, D. Zhang, E. C. Fortner, X. Tie, L. T. Molina and M. J. Molina, *Science*, 2004, **304**, 1487-1490.
31 J. Elm and K. V. Mikkelsen, *Chem. Phys. Lett.*, 2014, **615**, 26-29.
32 W. Xu and R. Zhang, *J. Phys. Chem. A*, 2012, **116**, 4539-4550.
33 W. Xu and R. Zhang, *J. Chem. Phys.*, 2013, **139**, 064312.
34 I. Ortega, O. Kupiainen, T. Kurtén, T. Olenius, O. Wilkman, M. McGrath, V. Loukonen and H. Vehkamäki, *Atmos. Chem. Phys.*, 2012, **12**, 225-235.
35 A. B. Nadykto, F. Yu, M. V. Jakovleva, J. Herb and Y. Xu, *Entropy*, 2011, **13**, 554-569.
36 T. Kurtén, V. Loukonen, H. Vehkamäki and M. Kulmala, *Atmos. Chem. Phys.*, 2008, **8**, 4095-4103.
37 V. Loukonen, T. Kurten, I. K. Ortega, H. Vehkamaki, A. A. H. Padua, K. Sellegri and M. Kulmala, *Atmos. Chem. Phys.*, 2010, **10**, 4961-4974.
38 J. Almeida, S. Schobesberger, A. Kürten, I. K. Ortega, O. Kupiainen-Määttä, A. P. Praplan, A. Adamov, A. Amorim, F. Bianchi and M. Breitenlechner, *Nature*, 2013, **502**, 359-363.
39 T. Berndt, F. Stratmann, M. Sipilä, J. Vanhanen, T. Petäjä, J. Mikkilä, A. Grüner, G. Spindler, L. Mauldin III and J. Curtius, *Atmos. Chem. Phys.*, 2010, **10**, 7101-7116.
40 W. Glasoe, K. Volz, B. Panta, N. Freshour, R. Bachman, D. Hanson, P. McMurry and C. Jen, *J. Geophys. Res. Atmos.*, 2015, **120**, 1933-1950.
41 C. N. Jen, P. H. McMurry and D. R. Hanson, *J. Geophys. Res. Atmos.*, 2014, **119**, 7502-7514.
42 M. Chen, M. Titcombe, J. Jiang, C. Jen, C. Kuang, M. L. Fischer, F. L. Eisele, J. I. Siepmann, D. R. Hanson and J. Zhao, *P. Natl. Acad. SCI. U.S.A.*, 2012, **109**, 18713-18718.
43 N. Freshour, K. Carlson, Y. Melka, S. Hinz, B. Panta and D. Hanson, *Atmos. Meas. Tech.*, 2014, **7**, 3611-3621.
44 D. Hanson, P. McMurry, J. Jiang, D. Tanner and L. Huey, *Environ. Sci. Technolo.*, 2011, **45**, 8881-8888.
45 V. Loukonen, T. Kurtén, I. Ortega, H. Vehkamäki, A. A. Padua, K. Sellegri and M. Kulmala, *Atmos. Chem. Phys.*, 2010, **10**, 4961-4974.
46 X. Ge, A. S. Wexler and S. L. Clegg, *Atmos. Environ.*, 2011, **45**, 561-577.
47 X. Ge, A. S. Wexler and S. L. Clegg, *Atmos. Environ.*, 2011, **45**, 524-546.
48 J. Zhao, J. Smith, F. Eisele, M. Chen, C. Kuang and P. McMurry, *Atmos. Chem. Phys.*, 2011, **11**, 10823-10836.
49 H. Yu and S.-H. Lee, *Environ. Chem.*, 2012, **9**, 190-201.
50 A. B. Nadykto, J. Herb, F. Yu and Y. Xu, *Chem. Phys. Lett.*, 2014, **609**, 42-49.
51 R. F. Bader, *Chem. Rev.*, 1991, **91**, 893-928.
52 P. Paasonen, T. Olenius, O. Kupiainen, T. Kurtén, T. Petäjä, W. Birmili, A. Hamed, M. Hu, L. Huey and C. Plass-Duelmer, *Atmos. Chem. Phys.*, 2012, **12**, 9113-9133.
53 H. Henschel, J. C. A. Navarro, T. Yli-Juuti, O. Kupiainen-Määttä, T. Olenius, I. K. Ortega, S. L. Clegg, T. Kurtén, I. Riipinen and H. Vehkamaki, *J. Phys. Chem. A*, 2014, **118**, 2599-2611.
54 J. Haywood and O. Boucher, *Rev. Geophys.*, 2000, **38**, 513-543.

55 D. J. Wales and J. P. K. Doye, *J. Phys. Chem. A*, 1997, **101**, 5111-5116.
56 S. Yoo and X. C. Zeng, *J. Chem. Phys.*, 2003, **119**, 1442-1450.
57 S. H. Yoo and X. C. Zeng, *Angew. Chem. Int. Edit.*, 2005, **44**, 1491-1494.
58 W. Huang, R. Pal, L. M. Wang, X. C. Zeng and L. S. Wang, *J. Chem. Phys.*, 2010, **132**, 054305.
59 W. Huang, H. J. Zhai and L. S. Wang, *J. Am. Chem. Soc.*, 2010, **132**, 4344-4351.
60 W. Huang and L.-S. Wang, *Phys. Rev. Lett.*, 2009, **102**, 153401.
61 W. Huang, A. P. Sergeeva, H.-J. Zhai, B. B. Averkiev, L.-S. Wang and A. I. Boldyrev, *Nat. Chem.*, 2010, **2**, 202-206.
62 W. Huang, M. Ji, C.-D. Dong, X. Gu, L.-M. Wang, X. G. Gong and L.-S. Wang, *ACS Nano*, 2008, **2**, 897-904.
63 L.-L. Yan, Y.-R. Liu, T. Huang, S. Jiang, H. Wen, Y.-B. Gai, W.-J. Zhang and W. Huang, *J. Chem. Phys.*, 2013, **139**, 244312.
64 Y.-R. Liu, H. Wen, T. Huang, X.-X. Lin, Y.-B. Gai, C.-J. Hu, W.-J. Zhang and W. Huang, *The J. Phys. Chem. A*, 2014, **118**, 508-516.
65 S.-S. Lv, Y.-R. Liu, T. Huang, Y.-J. Feng, S. Jiang and W. Huang, *J. Phys. Chem. A*, 2015, **119**, 3770-3779.
66 S. Jiang, T. Huang, Y.-R. Liu, K.-M. Xu, Y. Zhang, Y.-Z. Lv and W. Huang, *Phys. Chem. Chem. Phys.*, 2014, **16**, 19241-19249.
67 S. Jiang, Y. R. Liu, T. Huang, H. Wen, K. M. Xu, W. X. Zhao, W. J. Zhang and W. Huang, *J. Comput. Chem.*, 2014, **35**, 159-165.
68 S.-K. Miao, S. Jiang, J. Chen, Y. Ma, Y.-P. Zhu, Y. Wen, M.-M. Zhang and W. Huang, *RSC Advances*, 2015, **5**, 48638-48646.
69 S.-T. Pei, S. Jiang, Y.-R. Liu, T. Huang, K.-M. Xu, H. Wen, Y.-P. Zhu and W. Huang, *J. Phys. Chem. A*, 2015, **119**, 3035-3047.
70 X.-Q. Peng, Y.-R. Liu, T. Huang, S. Jiang and W. Huang, *Phys. Chem. Chem. Phys.*, 2015, **17**, 9552-9563.
71 Y.-P. Zhu, Y.-R. Liu, T. Huang, S. Jiang, K.-M. Xu, H. Wen, W.-J. Zhang and W. Huang, *J. Phys. Chem. A*, 2014, **118**, 7959-7974.
72 B. Delley, *J. Chem. Phys.*, 1990, **92**, 508-517.
73 M. Frisch, G. Trucks, H. B. Schlegel, G. Scuseria, M. Robb, J. Cheeseman, G. Scalmani, V. Barone, B. Mennucci and G. Petersson, *Inc., Wallingford, CT*, 2009, **270**, 271.
74 Y. Xu, A. B. Nadykto, F. Yu, L. Jiang and W. Wang, *J. Mol. Struct: THEOCHEM*, 2010, **951**, 28-33.
75 J. Herb, A. B. Nadykto and F. Yu, *Chem. Phys. Lett.*, 2011, **518**, 7-14.
76 J. Elm, M. Bilde and K. V. Mikkelsen, *J. Chem. Theory. Computat.*, 2012, **8**, 2071-2077.
77 W. Klopper, K. L. Bak, P. Jørgensen, J. Olsen and T. Helgaker, *J. Phys. B: At., Mol. Opt. Phys.*, 1999, **32**, R103.
78 A. Halkier, T. Helgaker, P. Jørgensen, W. Klopper, H. Koch, J. Olsen and A. K. Wilson, *Chem. Phys. Lett.*, 1998, **286**, 243-252.
79 A. Halkier, T. Helgaker, P. Jørgensen, W. Klopper and J. Olsen, *Chem. Phys. Lett.*, 1999, **302**, 437-446.
80 H. Werner, P. Knowles, G. Knizia, F. Manby, M. Schütz, P. Celani, T. Korona, R. Lindh, A. Mitrushenkov and G. Rauhut, *Cardiff University: Cardiff, UK*, 2010.
81 B. Temelso, T. E. Morrell, R. M. Shields, M. A. Allodi, E. K. Wood, K. N. Kirschner, T. C. Castonguay, K. A. Archer and G. C. Shields, *J. Phys. Chem. A*, 2012, **116**, 2209-2224.

82 J. G. Hill, *Int. J. Quantum Chem.*, 2013, **113**, 21-34.
83 J. R. Lane and H. G. Kjaergaard, *J. Chem. Phys.*, 2009, **131**, 034307.
84 J. Elm, P. Norman, M. Bilde and K. V. Mikkelsen, *Phys. Chem. Chem. Phys.*, 2014, **16**, 10883-10890.
85 S. Maheshwary, N. Patel, N. Sathyamurthy, A. D. Kulkarni and S. R. Gadre, *J. Phys. Chem. A*, 2001, **105**, 10525-10537.
86 E. R. Johnson, S. Keinan, P. Mori-Sanchez, J. Contreras-Garcia, A. J. Cohen and W. Yang, *J. Am. Chem. Soc.*, 2010, **132**, 6498-6506.
87 J. Contreras-García, W. Yang and E. R. Johnson, *J. Phys. Chem. A*, 2011, **115**, 12983-12990.
88 X. Yang, L. Gan, L. Han, E. Wang and J. Wang, *Angew. Chem.*, 2013, **125**, 2076-2080.
89 T. Lu and F. Chen, *J. Comput. Chem.*, 2012, **33**, 580-592. http://multiwfn.codeplex.com.
90 W. Humphrey, A. Dalke and K. Schulten, *J. Mol. Graphics*, 1996, **14**, 33-38. http://www.ks.uiuc.edu/Research/vmd/.
91 J. Kim, B. J. Mhin, S. J. Lee and K. S. Kim, *Chem. Phys. Lett.*, 1994, **219**, 243–246.
92 J. H. Seinfeld and S. N. Pandis, J. H. Seinfeld and S. N. Pandis, John Wiley & Sons Inc, Hoboken, New Jersey, 2012, pp. 691–711.
93 Y. Chan, R. Simpson, G. H. Mctainsh, P. D. Vowles, D. Cohen and G. Bailey, Atmos. Environ., 1999, **33**, 3237-3250.
94 E. Orestes, P. Chaudhuri and S. Canuto, *Mol. Phys.*, 2012, **110**, 297-306.
95 P. Chaudhuri and S. Canuto, *J. Mol. Struct: THEOCHEM*, 2006, **760**, 15-20.

Table 1 Calculated isotropic mean polarizabilities of H_2O, CH_3NHCH_3, $(CH_3NHCH_3)(H_2O)$, $(CH_3NHCH_3)(H_2O)_2$ using different DFT functionals with the aug-cc-pVDZ basis set.

Functional	H_2O	CH_3NHCH_3	$(CH_3NHCH_3)(H_2O)$	$(CH_3NHCH_3)(H_2O)_2$
B3LYP	9.472	39.481	49.087	58.787
PW91PW91	10.051	41.143	56.648	61.809
M06-2X	8.893	38.351	47.072	56.437
ωB97x-D	9.185	38.431	47.553	56.925
CAM-B3LYP	9.326	38.477	47.781	57.283
MP2	9.301	38.486	47.699	57.320

Table 2 A comparison of the changes at the DF-MP2-F12/CBS level in terms of ΔE (kcal/mol), ΔE+ZPE (kcal/mol), ΔH (kcal/mol), and ΔG (kcal/mol) associated with formation of the $(CH_3)_2NH(H_2O)_{n=1-4}$. The zero-point energy, thermal correction to enthalpy and Gibbs free energy were calculated from a vibration analysis at the PW91PW91/6-311++G (3df, 3pd) level (1 atm, 298K.)

Reaction	Isomer	ΔE	ΔE+ZPE	ΔH	ΔG
$(CH_3)_2NH+H_2O\leftrightarrow$	1a	-7.72	-5.63	-5.99	1.60
$(CH_3)_2N\bullet H_2O$	1b	-7.45	-5.43	-5.74	1.46
$(CH_3)_2N\bullet 1H_2O+H_2O\leftrightarrow$	2a	-9.04	-6.64	-7.41	2.25
$(CH_3)_2NH\bullet 2H_2O$	2b	-8.95	-6.53	-7.36	2.49
$(CH_3)_2N\bullet 2H_2O+H_2O\leftrightarrow$	3a	-10.48	-8.07	-9.04	1.02
$(CH_3)_2NH\bullet 3H_2O$	3b	-10.15	-7.95	-8.78	0.67
	3c	-10.02	-7.68	-8.61	1.25
	3d	-7.97	-5.28	-6.14	2.93
	3e	-7.76	-5.08	-5.94	3.07
	3f	-7.4	-4.77	-5.58	2.51
	3g	-7.11	-4.53	-5.31	2.81
	3h	-6.92	-4.27	-5.07	3.28
$(CH_3)_2NH\bullet 3H_2O+H_2O\leftrightarrow$	4a	-8.69	-6.64	-7.26	1.42
$(CH_3)_2NH\bullet 4H_2O$	4b	-8.17	-6.23	-6.76	1.65
	4c	-8.08	-6.16	-6.7	1.44
	4d	-8.41	-6.11	-6.85	3.11
	4e	-8.13	-6.1	-6.7	1.77
	4f	-8.16	-5.98	-6.56	2.75
	4g	-8.62	-5.88	-6.76	3.14
	4h	-8.52	-5.81	-6.61	1.14
	4i	-8.34	-5.67	-6.48	2.15
	4j	-7.81	-5.66	-6.17	2.72

Table 3 A comparison of the changes at the DF-MP2-F12/CBS level in terms of ΔE (kcal/mol), ΔE+ZPE (kcal/mol), ΔH (kcal/mol), and ΔG (kcal/mol) associated with formation of the $(CH_3)_2NH(H_2O)_{n=5-6}$. The zero-point energy, thermal correction to enthalpy and Gibbs free energy were calculated from a vibration analysis at the PW91PW91/6-311++G (3df, 3pd) level.

Reaction	Isomer	ΔE	ΔE+ZPE	ΔH	ΔG
$(CH_3)_2NH•4H_2O+H_2O\leftrightarrow$ $(CH_3)_2NH•5H_2O$	5a	-10.36	-7.68	-8.66	2.64
	5b	-9.91	-6.83	-7.92	3.35
	5c	-9.41	-6.77	-7.69	2.67
	5d	-9.51	-6.72	-7.62	2.18
	5e	-9.31	-6.47	-7.44	2.87
	5f	-8.91	-6.3	-7.22	2.94
	5g	-8.53	-5.96	-6.85	3.26
	5h	-8.38	-5.94	-6.84	3.32
	5i	-8.54	-5.72	-6.62	2.4
	5j	-8.28	-5.55	-6.36	2.68
	5k	-8.25	-5.48	-6.88	3.89
	5l	-8.23	-5.44	-6.27	2.01
	5m	-7.94	-5.14	-5.96	2.36
	5n	-7.24	-4.85	-5.52	3.85
	5o	-7.58	-4.54	-5.27	2.79
	5p	-7.3	-4.34	-5.21	3.82
	5q	-7.26	-4.31	-5.14	3.55
	5r	-7.22	-3.99	-4.85	3.79
$(CH_3)_2NH•5H_2O+H_2O\leftrightarrow$ $(CH_3)_2NH•6H_2O$	6a	-11.64	-10.88	-9.64	0.80
	6b	-11.37	-10.23	-9.09	1.58
	6c	-9.68	-9.18	-7.68	1.52
	6d	-8.74	-8.88	-7.26	2.18
	6e	-9.40	-8.63	-7.33	2.55
	6f	-8.93	-8.48	-7.76	4.48
	6g	-7.56	-8.40	-6.78	2.59
	6h	-8.25	-8.14	-6.67	3.16
	6i	-8.54	-7.66	-6.12	1.85
	6j	-7.61	-7.51	-5.83	1.46
	6k	-8.44	-7.45	-5.98	2.20
	6l	-8.01	-7.30	-5.75	2.15
	6m	-7.17	-7.08	-5.33	1.66
	6n	-7.39	-7.07	-5.38	2.98
	6o	-7.71	-7.02	-5.44	2.31

Figure Captions

Figure. 1 A comparison of the differences between the binding energies for six isomers of $(CH_3)_2NH(H_2O)_{n=1,2,3}$ at the DF-MP2-F12/X level and DF-MP2-F12/VQZ-F12 level.

Figure. 2 The global minimum and the local minima for $(CH_3)_2NH(H_2O)_{n=1-3}$ optimized at the PW91PW91/6-311++G(3df, 3pd) level. The relative energies (kcal/mol) with the respect to the most stable structure are given in the parentheses.

Figure. 3 The global minimum and the local minima for $(CH_3)_2NH(H_2O)_4$ optimized at the PW91PW91/6-311++G(3df, 3pd) level. The relative energies (kcal/mol) with the respect to the most stable structure are given in the parentheses.

Figure. 4 The global minimum and the local minima for $(CH_3)_2NH(H_2O)_5$ optimized at the PW91PW91/6-311++G(3df, 3pd) level. The relative energies (kcal/mol) with the respect to the most stable structure are given in the parentheses.

Figure. 5 The global minimum and the local minima for $(CH_3)_2NH(H_2O)_6$ optimized at the PW91PW91/6-311++G(3df, 3pd) level. The relative energies (kcal/mol) with the respect to the most stable structure are given in the parentheses.

Figure. 6 The lowest-energy structures and the isosurfaces (s =0.5 a.u) of the $(CH_3)_2NH(H_2O)_6$ clusters at the PW91PW91/6-311++G(3df, 3pd) level are given.

Figure. 7 A comparison of the global minimum binding energies, enthalpies and Gibbs free energies of the stepwise DMA hydrate growth at DF-MP2-F12/CBS (limit DZ, TZ) level [$(CH_3)_2NH(H_2O)_{n-1} + H_2O \rightarrow (CH_3)_2NH(H_2O)_n$].

Figure. 8 The conformational population changes for the low isomers of $(CH_3)_2NH(H_2O)_{1-6}$ versus the temperature: (8a) $(CH_3)_2NH(H_2O)_{1,2}$; (8b)

$(CH_3)_2NH(H_2O)_3$; (8c) $(CH_3)_2NH(H_2O)_4$; (8d) $(CH_3)_2NH(H_2O)_5$, (8e) $(CH_3)_2NH(H_2O)_6$.

Figure. 9 The Gibbs free energy changes (in kcal/mol) for the minimum thermodynamics of stepwise hydration of $(CH_3)_2NH(H_2O)_{n=1-6}$ clusters at different temperature.

Figure. 10 The Rayleigh light scattering and cluster polarizability properties: (9a) isotropic mean polarizabilities as a function of water molecules; (9b) Rayleigh light scattering intensities as the function of water molecules; (9c) anisotropic polarizabilities as a function of water molecules; (9d) depolarization ratio as a function of water molecules.

Figure. 1

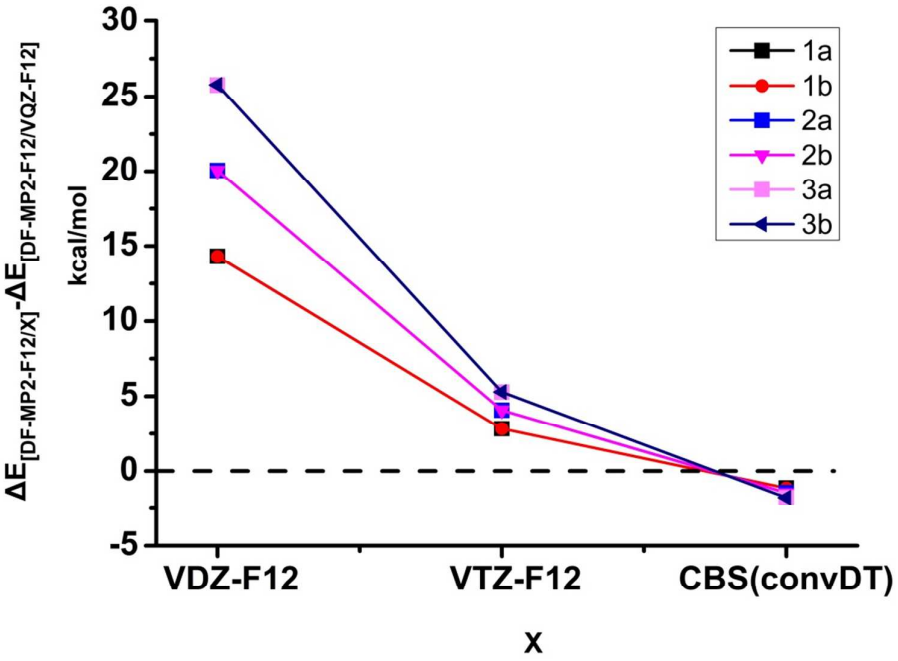

Figure. 2

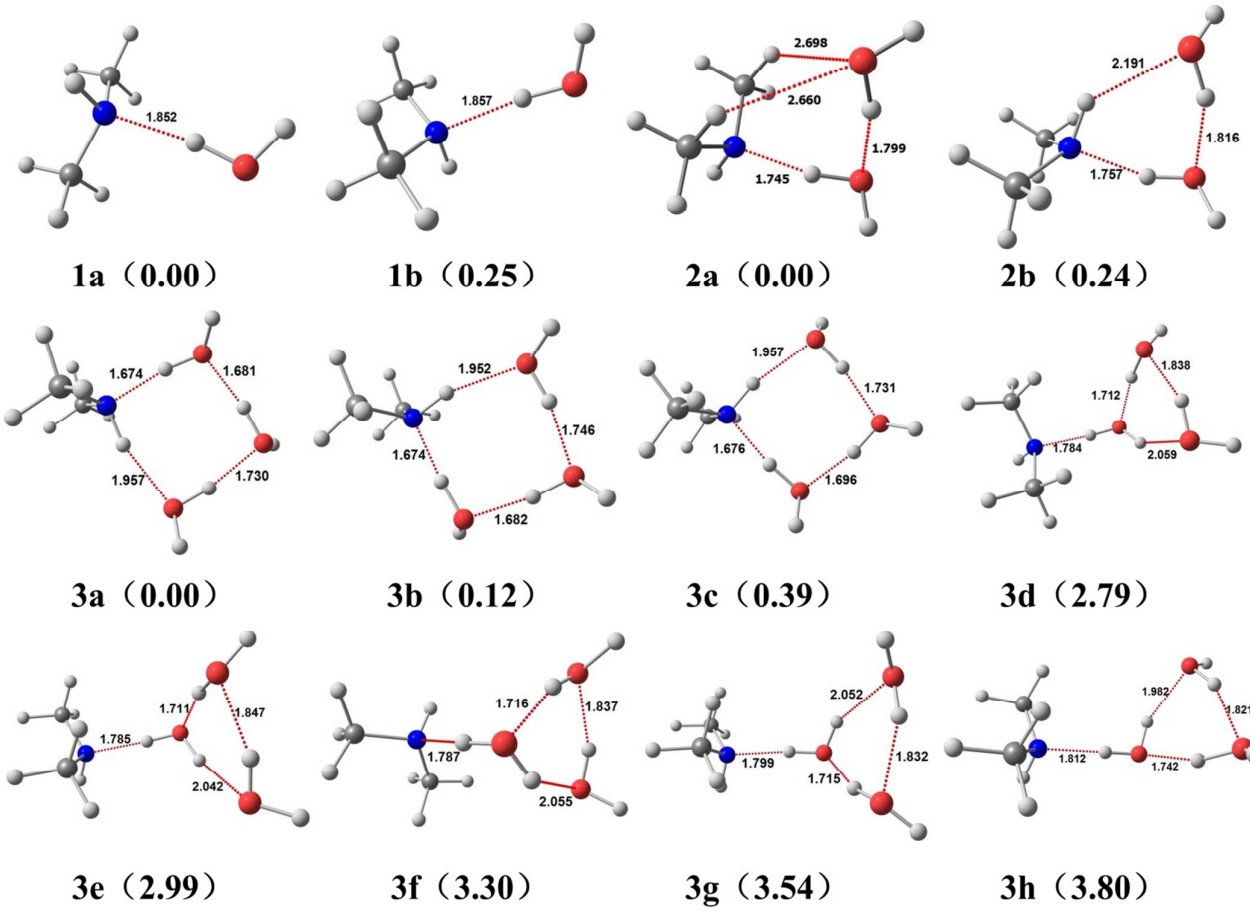

Figure. 3

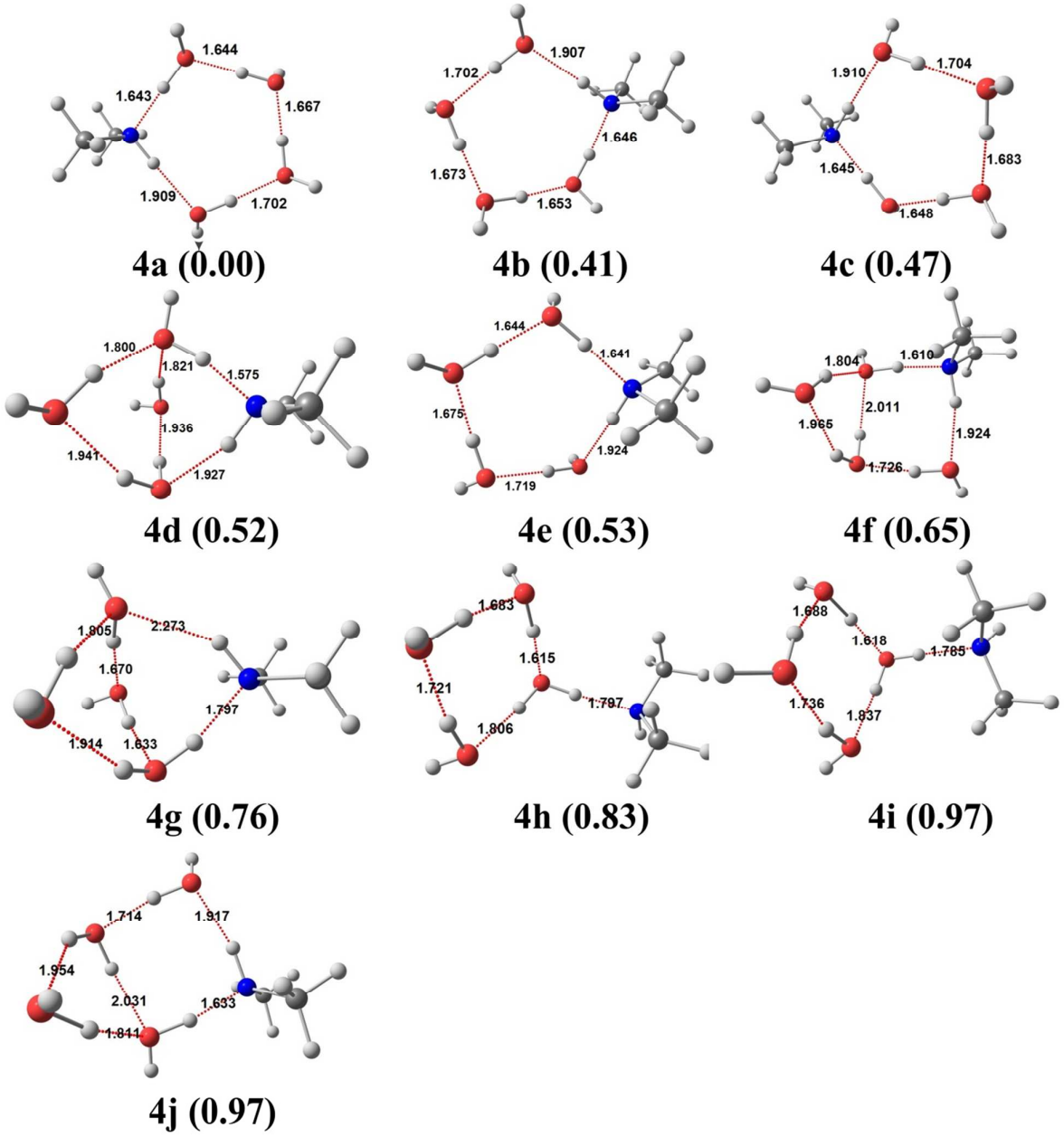

Figure. 4

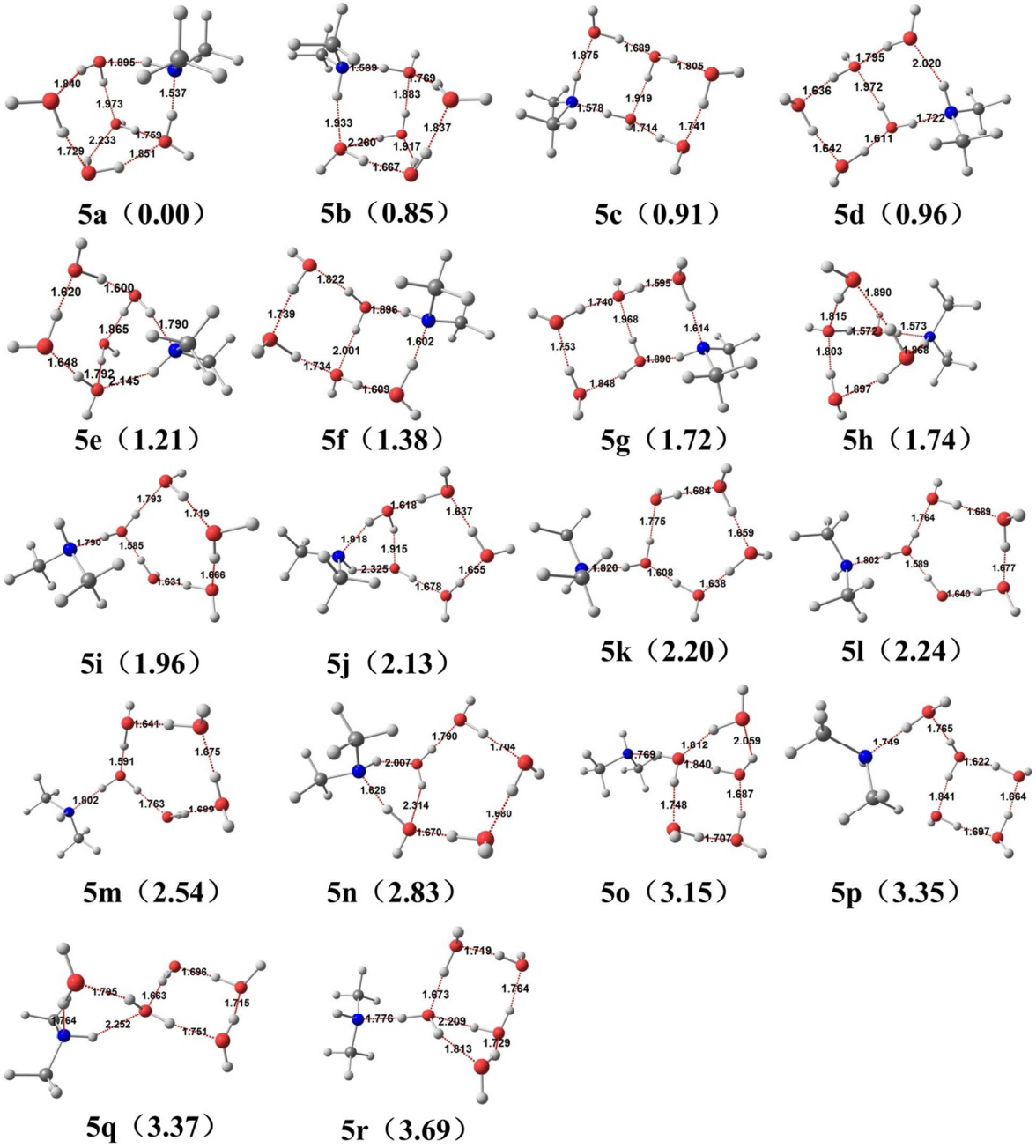

Figure. 5

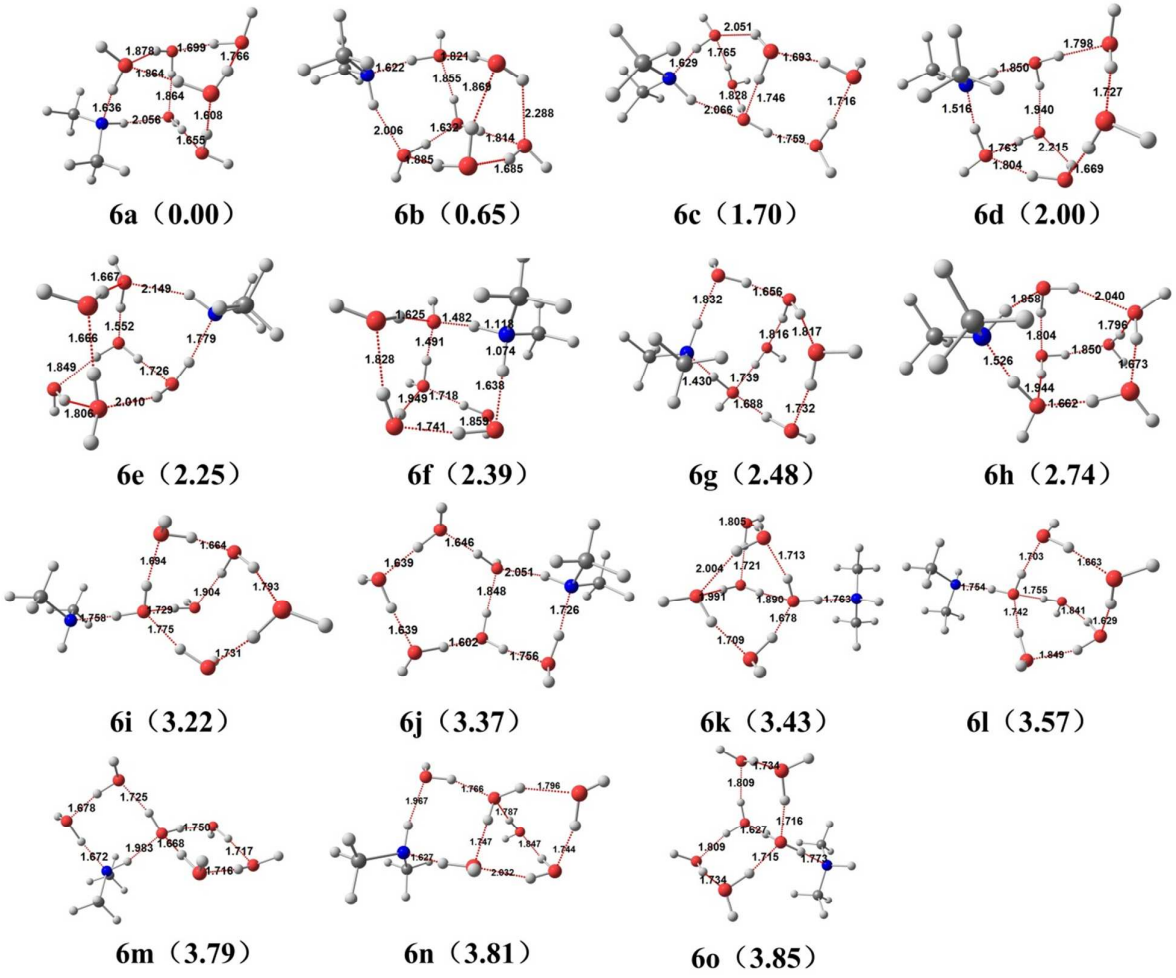

Figure. 6

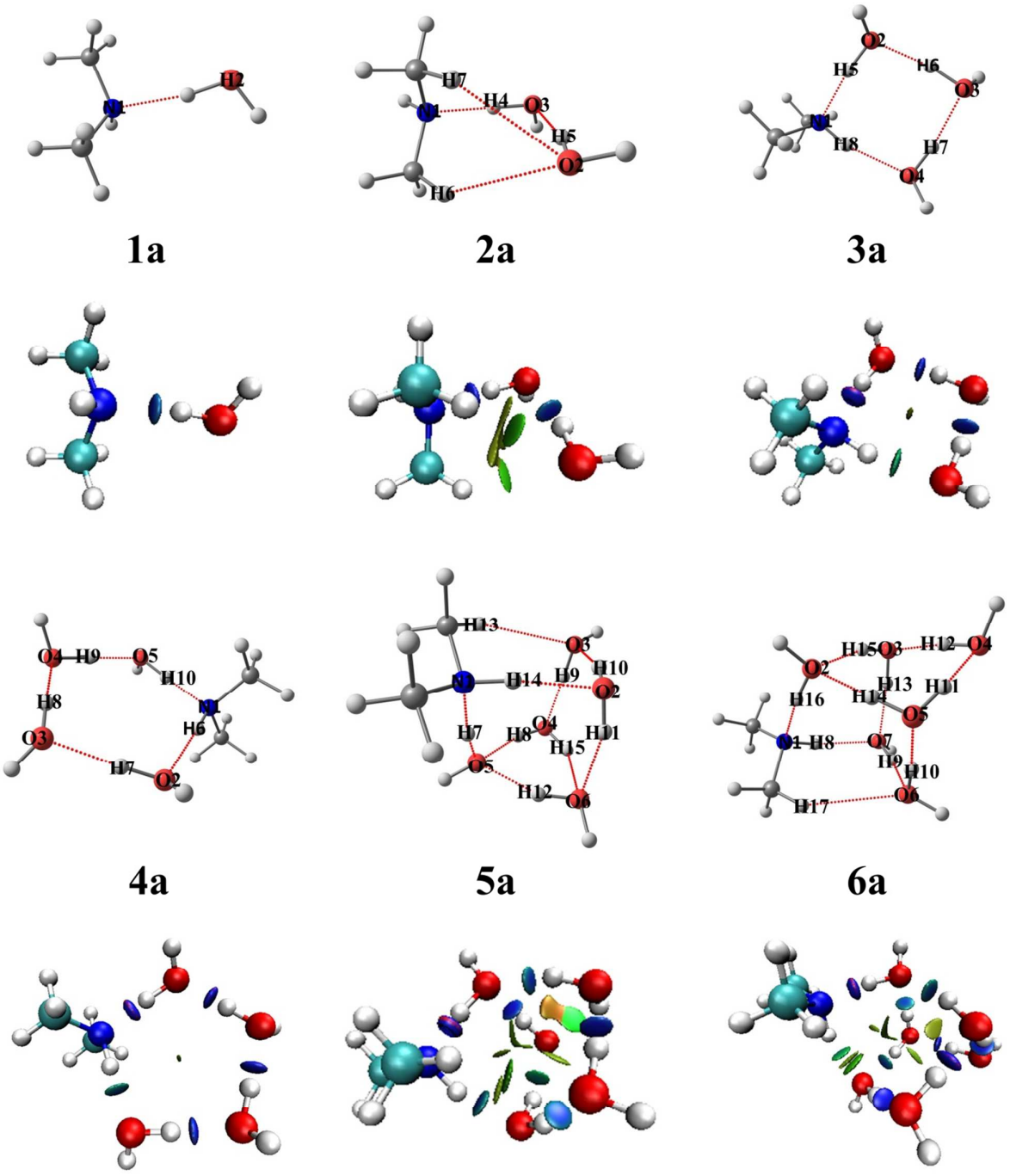

Figure. 7

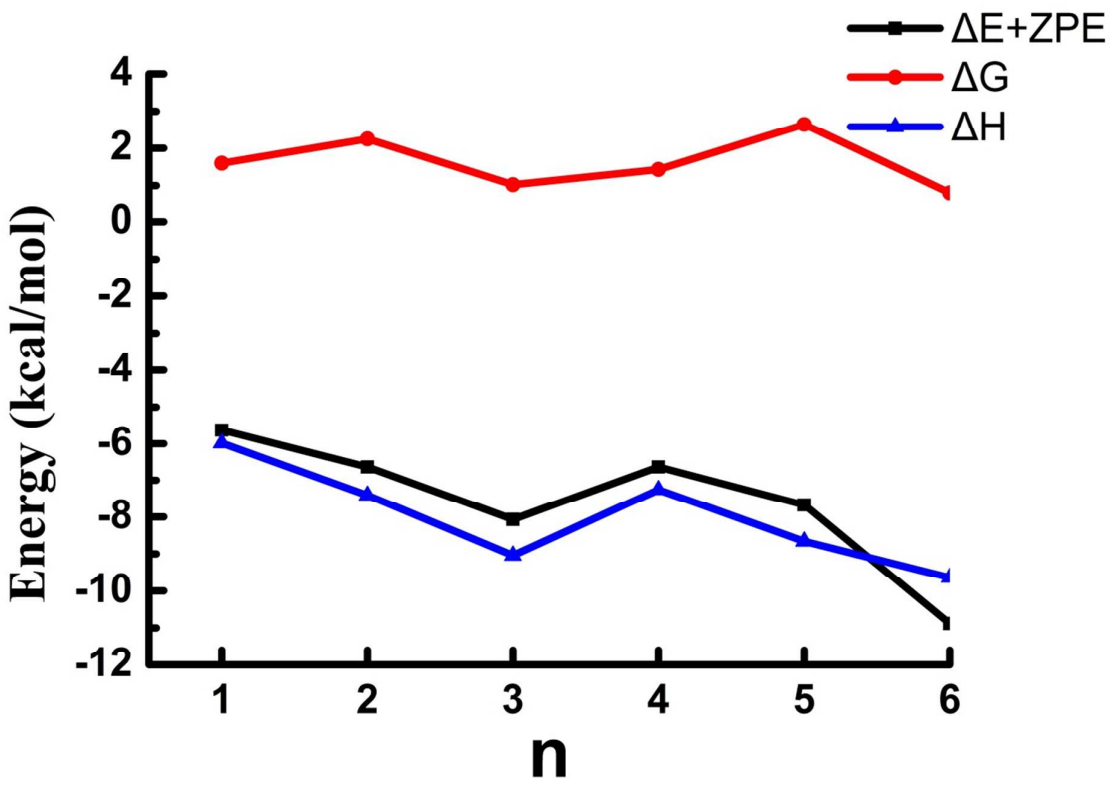

Figure. 8

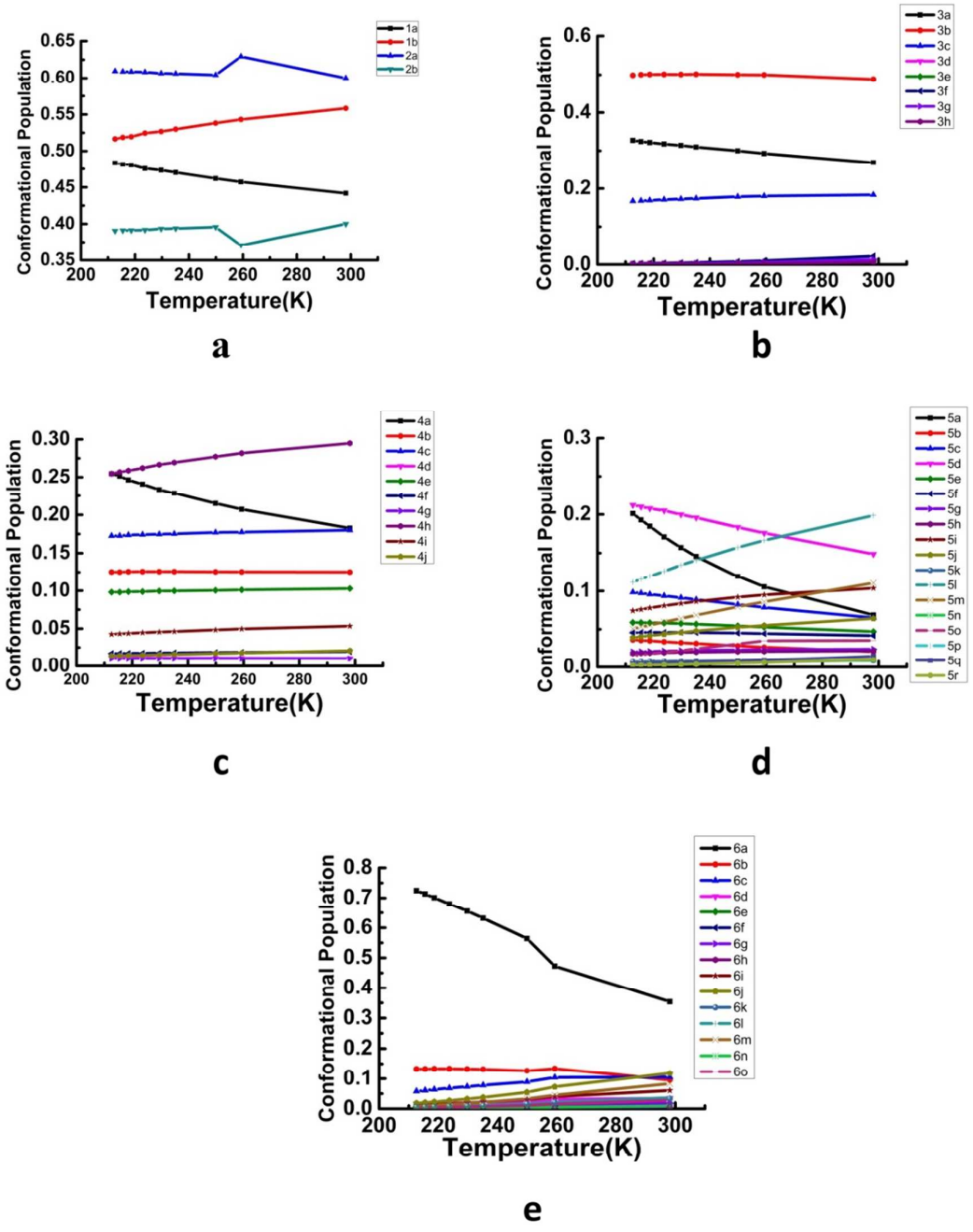

Figure. 9

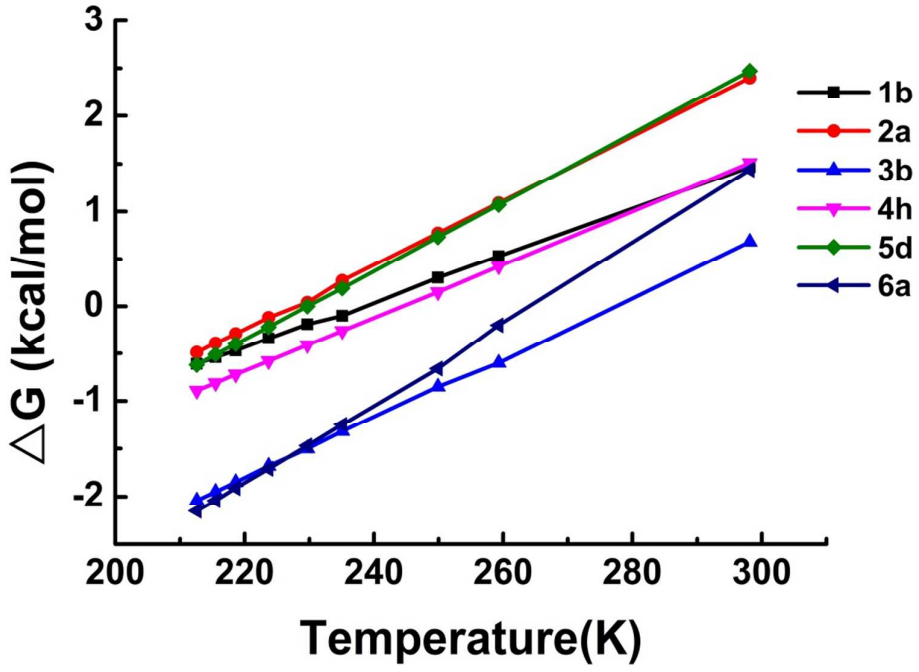

Figure. 10